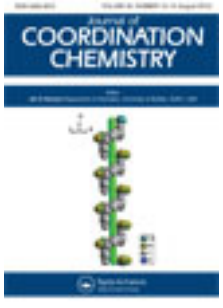

Journal of Coordination Chemistry
Publication details, including instructions for authors and subscription information:
http://www.tandfonline.com/loi/gcoo20

Crystal structure and interaction with bovine serum albumin of the Cu(I/II) complex $[C_{20}H_{32}Cu_2I_3N_4]_n$

Yu-Fen Liu [a], Hai-Tao Xia [a] & De-Fu Rong [b]
[a] School of Chemical Engineering, Huaihai Institute of Technology, Lianyungang, Jiangsu, China
[b] Beilun Entry-Exit Inspection and Quarantine Bureau of China, Ningbo, Zhejiang, China
Accepted author version posted online: 25 Jun 2012.Published online: 10 Jul 2012.

To cite this article: Yu-Fen Liu, Hai-Tao Xia & De-Fu Rong (2012) Crystal structure and interaction with bovine serum albumin of the Cu(I/II) complex $[C_{20}H_{32}Cu_2I_3N_4]_n$, Journal of Coordination Chemistry, 65:16, 2919-2934, DOI: 10.1080/00958972.2012.706282

To link to this article: http://dx.doi.org/10.1080/00958972.2012.706282

Journal of Coordination Chemistry
Vol. 65, No. 16, 20 August 2012, 2919–2934

Crystal structure and interaction with bovine serum albumin of the Cu(I/II) complex $[C_{20}H_{32}Cu_2I_3N_4]_n$

YU-FEN LIU†, HAI-TAO XIA*† and DE-FU RONG‡

†School of Chemical Engineering, Huaihai Institute of Technology, Lianyungang, Jiangsu, China
‡Beilun Entry-Exit Inspection and Quarantine Bureau of China, Ningbo, Zhejiang, China

(*Received 19 January 2012; in final form 8 May 2012*)

$[C_{20}H_{32}Cu_2I_3N_4]_n$ was synthesized and characterized by elemental analysis, ESI-MS spectrometry, and IR spectra. The crystal structure was determined by X-ray single-crystal diffraction. The binding of the complex with bovine serum albumin (BSA) was studied by fluorescence spectroscopy under simulated physiological conditions. The binding constant (K_b), the number of binding sites (n), and the corresponding thermodynamic parameters ΔH, ΔS, ΔG were calculated based on the van't Hoff equation. The complex had strong ability to quench the fluorescence from BSA, and the quenching mechanism of this complex to BSA was static quenching. Hydrogen bonds and van der Waals forces are the interactions between the Cu(I/II) complex and BSA. According to the Förster non-radiation energy transfer theory, the binding average distance between the donor (BSA) and the acceptor (Cu(I/II) complex) was obtained. The effect of the complex on the BSA conformation was also studied by using synchronous fluorescence spectroscopy.

Keywords: Cu(I/II) Complex; Crystal structure; Bovine serum albumin; Fluorescence spectrum

1. Introduction

Copper is a physiologically important metal [1, 2], playing an important role in growth, scavenging harmful free radicals, and preventing oxidative damage to cells, protein synthesis, and the activity of metal enzymes [3], capable of participating in a variety of redox cycling reactions [4]. Protein is the major target of many types of medicines. Studying the structure and function of proteins are important in biochemistry, chemistry, and medicine. Serum albumins are the most abundant proteins in the circulatory system with many important physiological functions, contributing to the osmotic blood pressure and mainly responsible for the maintenance of blood pH [5–7]. The most important physiological role of albumins is the binding, transport, and deposition of a variety of endogenous and exogenous substances in blood [8], such as fatty acids, drugs, metabolites, metal ions, and other biologically-active compounds present in the blood [9]. Distribution, free concentration, and metabolism of various

*Corresponding author. Email: xht161006@hhit.edu.cn

Journal of Coordination Chemistry
ISSN 0095-8972 print/ISSN 1029-0389 online
http://dx.doi.org/10.1080/00958972.2012.706282

drugs can be significantly altered as a result of their binding to serum albumin [10]. Thus, investigating the interaction between serum albumins and drugs is important for understanding the transportation and distribution of drugs in the body and clarifying the action mechanism and pharmaceutical dynamics, important in chemistry, life sciences, and clinical medicine. Among the serum albumins, bovine serum albumin (BSA) is usually selected as the protein model because of its abundance, low cost, ease of purification, stability, medical importance, and unusual ligand-binding properties. Studies are consistent with the fact that human and BSAs are homologous proteins [11, 12]. Techniques used to detect the interaction between drugs and serum albumin include fluorescence spectroscopy [8, 13–15], UV-spectrophotometry [16, 17], Fourier transform infrared (FT-IR) [18, 19], circular dichroism spectroscopy, and cyclic voltammetry [20, 21]; fluorescence quenching is a useful method to study the reactivity of chemical and biological systems since it allows non-intrusive measurements of substances in low concentration under physiological conditions [22]. It can reveal accessibility of quenchers to serum albumin's fluorophores, help in understanding binding mechanisms of serum albumin to compounds, and provide clues to the nature of the binding phenomenon. Despite the numerous studies on copper complexes and their interactions with bio-macromolecules [23–25], in this study, we report the crystal structure of a new copper (I/II) complex containing N^1-benzylpropane-1,2-diamine. The binding properties of this complex with BSA have been carried out using fluorescence spectroscopy, giving binding constants at different temperatures in HCl-Tris (pH 7.4) buffer solution. The enthalpy changes (ΔH) and entropy changes (ΔS) between BSA and the complex are calculated and the interaction between BSA and the complex are discussed.

2. Experimental

2.1. *Materials*

BSA was purchased from Beijing Biosea Biotechnology Company; its molecular weight is assumed to be 67000. All BSA solutions are prepared in a pH 7.4 buffer solution, and BSA stock solution (1.0×10^{-4} mol L^{-1}) was kept in the dark at 4°C. NaCl (analytical grade, 0.5 mol L^{-1}) is used to maintain the ionic strength. Buffer solution consist of Tris (0.05 mol L^{-1}) and HCl (0.05 mol L^{-1}), and the pH is adjusted to 7.4 by adding 0.1 mol L^{-1} NaOH at 298 K. The Cu(I/II) complex solutions (3.0×10^{-5} mol L^{-1}) were prepared in ethanol. All other materials were of analytical reagent grade; solutions are prepared with doubly-distilled water.

2.2. *Physical measurements*

Elemental analyses were measured on a Perkin-Elmer 2400c Element analyzer. Infrared spectra were recorded on a Nicolet 5DX FT-IR spectrophotometer using KBr discs from 4000 to 400 cm^{-1}. Fluorescence spectra were measured with a Shimadzu RF-5301 fluorophotometer equipped with a 150 W Xenon lamp source and 1.0 cm quartz cell. Absorption spectra were studied with a Shimadzu UV-2550 PC spectrophotometer. MS spectra were recorded on a Shimadzu LCMS-2020 mass spectrometer using ethanol as mobile phase.

2.3. *Preparation of ligand*

To a solution of benzaldehyde (0.1 mol) in ethanol (20 mL), propane-1,2-diamine (0.1 mol) in ethanol (20 mL) was added. The mixed solution was stirred for 5 h at 70°C, allowed to stand, and the precipitate was collected by filtration. The precipitate was dissolved in 40 mL ethanol : chloroform (1 : 2 v/v) and solid $NaBH_4$ (0.4 mol) was added. The mixture was stirred at 45°C for 7 h and then water was added to 200 mL, statically separated, the yellow viscous liquid was obtained by evaporating the organic solvent. Anal. Calcd for $C_{10}H_{16}N_2$ (%): C, 73.12; H, 9.82; N, 17.06. Found (%): C, 73.45; H, 9.77; N, 17.09. IR (KBr, ν (cm^{-1})): 3306, 3034, 2968, 2812, 1603, 1545, 1451, 1154, 1025, 732, 693.

2.4. *Preparation of complex*

To a solution of the ligand (10 mmol) in methanol (30 mL), a mixture of $CuAc_2$ (5 mmol) and NaI (5 mmol) in water (10 mL) was added. The mixture was stirred at 70°C for 2 h and the color of the solution turned gradually green. The solvent was cooled to room temperature, a green precipitate was collected by filtration, washed with water and methanol successively, and finally dried to afford green powder in 67.9% yield. Recrystallization of the complex from ethanol at room temperature gave crystals suitable for X-ray single-crystal diffraction. Anal. Calcd for $C_{20}H_{32}Cu_2I_3N_4$ (%): C, 28.72; H, 3.86; N, 6.70. Found (%): C, 28.45; H, 3.73; N, 6.72. IR (KBr, ν (cm^{-1})): 3440, 2924, 2852, 1637, 1494, 1450, 1384, 1230, 1070, 765, 700, 617, 557. ESI-MS (m/z): 881.6, 838.5, 707.9, 673.9, 415.3, 372.9, 291.8, 279.1, 198.1.

2.5. *X-ray crystal structure determination*

A single-crystal of the complex suitable for X-ray crystallographic analysis was mounted in sealed glass capillaries. Diffraction data were collected with a Bruker SMART 1000 CCD diffractometer by the use of graphite monochromated Mo-Kα radiation ($\lambda = 0.71073$ Å) at 298(2) K. The crystal structure was solved by direct methods and all non-hydrogen atoms were located with successive difference Fourier syntheses. The structure was refined by full-matrix least-squares on F^2 with anisotropic thermal parameters for all non-hydrogen atoms. Hydrogen atoms were added according to theoretical models. All calculations were performed using the programs contained in the SHELXL package [26, 27]. A summary of crystallographic data and refinement parameters for the Cu(I/II) complex are given in table 1.

2.6. *Fluorescence spectra*

The fluorescence measurements of complex-BSA solutions were performed at different temperatures by keeping the concentration of BSA fixed at 3×10^{-6} mol L^{-1} while varying the Cu(I/II) complex concentration from 0 to 7×10^{-6} mol L^{-1}. The widths of both the excitation slit and the emission slit were set to 5.0 nm. Fluorescence spectra were recorded from 300 to 500 nm at an excitation wavelength of 285 nm.

Table 1. Crystal data and structure refinement for complex.

Formula	$C_{20}H_{32}N_4Cu_2\ I_3$
Formula weight	836.28
Temperature (K)	293(2)
Wavelength (Å)	0.71073
Crystal system	Monoclinic
Space group	*P2(1)*
Unit cells and dimensions (Å, °)	
a	9.8764(15)
b	13.4861(19)
c	10.6808(18)
α	90
β	103.892(2)
γ	90
Volume (Å^3), *Z*	1381.0(4), 2
Calculated density (Mg m^{-3})	2.011
F(000)	794
Crystal size (mm^3)	$0.31 \times 0.30 \times 0.29$
θ Range for data collection (°)	1.96–25.01
Reflections collected	6877
Independent reflection	4781 [R(int) = 0.0491]
Refinement method	Full-matrix least-squares on F^2
Data/restraints/parameters	4781/1/331
Goodness-of-fit on F^2	0.99
Final R indices [$I > 2\sigma(I)$]	$R_1 = 0.0579$, $wR_2 = 0.1306$
Largest difference peak and hole (e Å^{-3})	0.810 and −0.694

2.7. *Energy transfer between protein and Cu(I/II) complex*

The absorption spectrum of the Cu(I/II) complex was recorded at 298 K from 300 to 500 nm (three replicates). The emission spectrum of BSA was also recorded at 298 K in the same range (three replicates). Then, the overlap of the UV absorption spectrum of complex with the fluorescence emission spectrum of BSA was used to calculate the energy transfer.

2.8. *Synchronous fluorescence spectra*

Synchronous fluorescence spectra were collected with $\Delta\lambda = 15$ and $\Delta\lambda = 60$ nm, respectively, under the same experimental conditions.

3. Results and discussion

3.1. *Crystal structure of complex*

The molecular structure of the complex is shown in figure 1 and selected bond distances, bond angles, and hydrogen bonds are summarized in table 2. The Cu(I/II) complex contains a dinuclear unit, an iodide bridges the pair of coppers, resulting in the formation of a polymer. Copper(II) is six-coordinate with a distorted octahedral

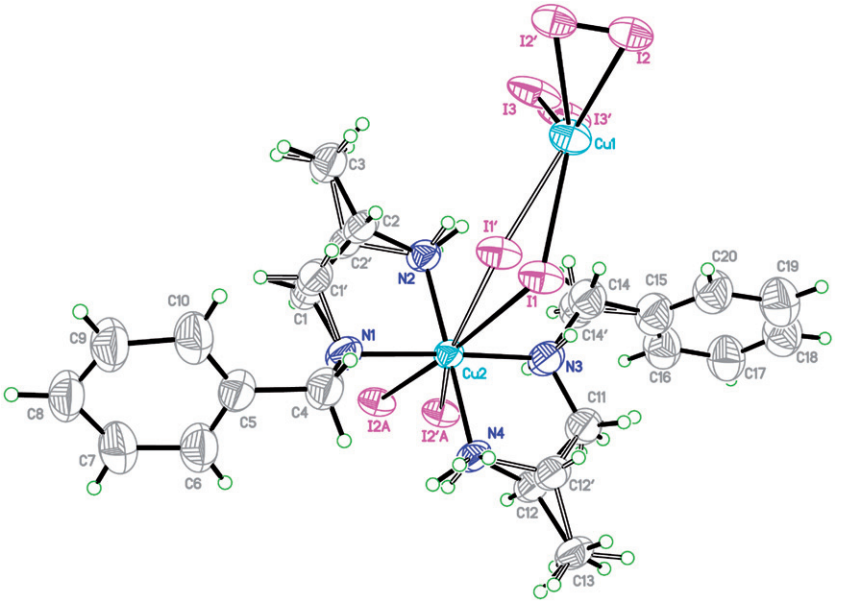

Figure 1. Molecular crystal structure of the Cu(I/II) complex [symmetry code: A $(1-x, -1/2+y, 1-z)$].

coordination geometry; the coordination atoms are four nitrogen atoms from two ligands and two iodides. The distortion leads to I–Cu–I angles ranging from 163(3)° to 171.31(17)°. The ligand donors are in the equatorial position with axial positions occupied by iodides. The Cu2–N distances are all different, ranging from 1.979(14) to 2.054(17) Å, shorter than that found for $[Cu_{0.92}Zn_{0.08}I_2(C_5H_5N)_4]\cdot 2C_5H_5N$ [28] (average Cu–N 2.037 Å) and longer than that for Cu–N $(Cu_3L_2(MeCN)_2I_2](MeCN)_2$, average 2.008 Å) [29]. The average Cu2–I distance is 3.277 Å, slightly longer than that [29] of (Cu2–I1 3.211(1) Å) and significantly shorter than that [28] of (Cu1–I1 3.460(5) Å). The copper(I) is three-coordinate with three iodides and exhibits a triangle planar arrangement with angles close to 120° (sum of the three angles = 359.7°). The Cu1–I bond lengths range from 2.463(19) to 2.577(5) Å, shorter than those reported for copper(I) iodide complexes [30–34]. Hydrogen atoms attached to N, C1, C2, C3, C11, C12, C13 and C1, C2, C11, C12 are disordered over two sites; the site occupancies are refined to 0.56(15) and 0.44(15), respectively. The I1, I2, and I3 are also disordered over two sites with site occupancies refined to 0.04(3) and 0.96(3), 0.985(5) and 0.015(5), 0.71(14) and 0.29(14), respectively.

There is one N–H $\cdots$ I and one C–H $\cdots$ *Cg* intramolecular hydrogen bond in the structure of the Cu(I/II) complex. The Cu(I) and Cu(II) units are linked into 1-D polymer chains parallel to the *b*-axis by I1, I2 atoms, and C10—H10 $\cdots$ *Cg* hydrogen bonds (center of ring C15 to C20) shown in figure 2. Adjacent polymer chains are linked into sheets parallel to the [001] plane by N4–H4B $\cdots$ $I3^{iii}$ hydrogen bonds shown in figure 3, and neighboring [001] sheets are linked into a 3-D network structure through van der Waals forces.

Table 2. Selected bond lengths (Å), hydrogen bond lengths (Å) and bond angles (°) for complex.

Cu1–I3′	2.463(19)	Cu2–N4	1.998(14)
Cu1–I1′	2.47(5)	Cu2–N3	2.018(17)
Cu1–I2′	2.53(9)	Cu2–N1	2.054(17)
Cu1–I2	2.558(3)	Cu2–I2′^{i}	3.18(9)
Cu1–I3	2.56(3)	Cu2–I1′	3.28(6)
Cu1–I1	2.577(5)	Cu2–I1	3.299(4)
Cu2–N2	1.979(14)	Cu2–I2	3.357(3)
I3′–Cu1–I1′	116.0(16)	N3–Cu2–I2′^{i}	68(2)
I3′–Cu1–I2′	120(4)	N1–Cu2–I2′^{i}	109(2)
I1′–Cu1–I2′	110(5)	N2–Cu2–I1′	78(4)
I3′–Cu1–I2	122.7(12)	N4–Cu2–I1′	101(4)
I1′–Cu1–I2	120.6(15)	N3–Cu2–I1′	98(5)
I2′–Cu1–I2	29(3)	N1–Cu2–I1′	85(5)
I3′–Cu1–I3	16(3)	I2′^{i}–Cu2–I1′	163(3)
I1′–Cu1–I3	116(3)	N2–Cu2–I1	87.5(5)
I2′–Cu1–I3	108(3)	N4–Cu2–I1	92.0(5)
I2–Cu1–I3	117.9(8)	N3–Cu2–I1	85.5(6)
I3′–Cu1–I1	116(2)	N1–Cu2–I1	96.8(6)
I1′–Cu1–I1	19(7)	I2′^{i}–Cu2–I1	154(2)
I2′–Cu1–I1	120(2)	I1′–Cu2–I1	15(5)
I2–Cu1–I1	120.43(11)	N2–Cu2–I2^{i}	85.8(5)
I3–Cu1–I1	121.4(6)	N4–Cu2–I2^{i}	94.8(5)
N2–Cu2–N4	178.6(7)	N3–Cu2–I2^{i}	90.0(6)
N2–Cu2–N3	97.8(6)	N1–Cu2–I2^{i}	88.0(6)
N4–Cu2–N3	83.5(6)	I2′^{i}–Cu2–I2^{i}	22(2)
N2–Cu2–N1	83.9(6)	I1′–Cu2–I2^{i}	163(5)
N4–Cu2–N1	94.8(6)	I1–Cu2–I2^{i}	171.31(8)
N3–Cu2–N1	177.2(8)	Cu1–I1–Cu2	109.70(17)
N2–Cu2–I2′^{i}	94.3(16)	Cu1–I2–Cu2^{ii}	106.65(8)
N4–Cu2–I2′^{i}	86.7(16)		

D–H···A	D–H	H···A	D···A	∠D–H···A
N4–H4B···I3^{iii}	0.9	2.76	3.62(2)	161
C10–H10···*Cg*^{ii}	0.93	2.92	3.75(3)	149

Symmetry codes: $^{i}1-x, -1/2+y, 1-z$; $^{ii}1-x, 1/2+y, 1-z$; $^{iii}-1+x, y, z$. *Cg* (center of ring C15–C20).

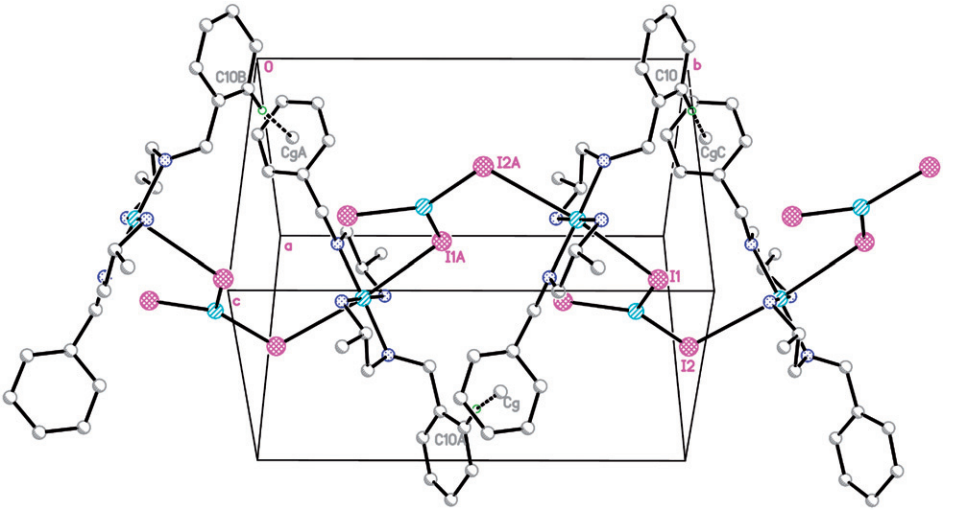

Figure 2. CH···*Cg* hydrogen bond contacts of Cu(I/II) complex [symmetry code: A $(1-x, -1/2+y, 1-z)$, B$(x, -1+y, z)$, C$(1-x, 1/2+y, 1-z)$].

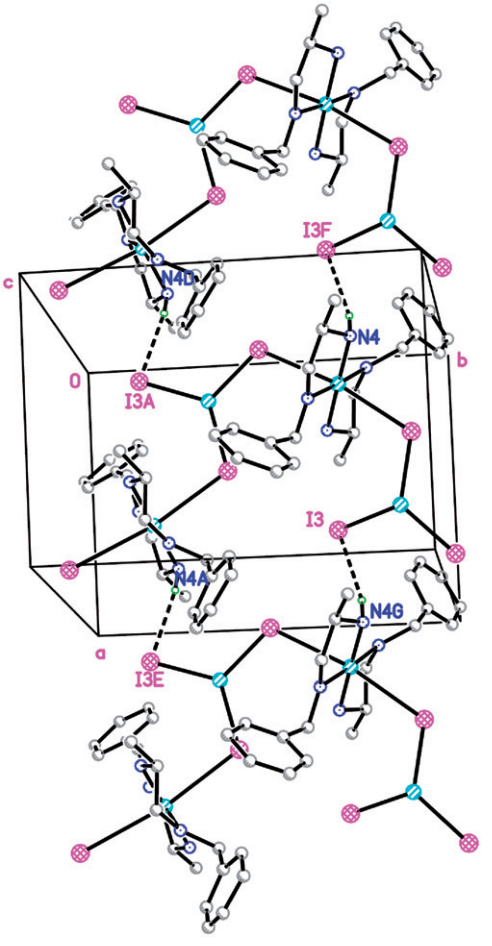

Figure 3. The N–H···I hydrogen bond contacts of Cu(I/II) complex [symmetry code: A $(1-x, -1/2+y, 1-z)$, D$(-x, -1/2+y, 1-z)$, E$(2-x, -1/2+y, 1-z)$, F$(-1+x, y, z)$, G$(1+x, y, z)$].

3.2. *ESI-MS and fluorescence spectroscopy*

ESI-MS was used to verify the solution phase stability of the Cu(I/II) complex. The 0.5 µL sample ethanol solution (10^{-5} mol L^{-1}) was injected into the electrospray source at a flow rate of 0.5 mL min^{-1}, probe voltage 4.5 kV (positive mode), nebulizing gas flow 1.5 L min^{-1}, drying gas pressure 0.1 MPa, temperatures of MS source block and probe were set at 200°C and 300°C, respectively. ESI mass spectra and the structural assignments for Cu(I/II) complex are shown in figure 4. The results show that the Cu(I/II) complex is stable in ethanol.

Fluorescence measurements give information about the molecular environment in the vicinity of the fluorophore molecules. The BSA molecule has three intrinsic fluorophores, tryptophan, tyrosine, and phenylalanine residues. Generally, BSA solutions excited at 285–290 nm emit fluorescence, attributable mainly to the tryptophan residues. A valuable feature of the intrinsic fluorescence of proteins is the high

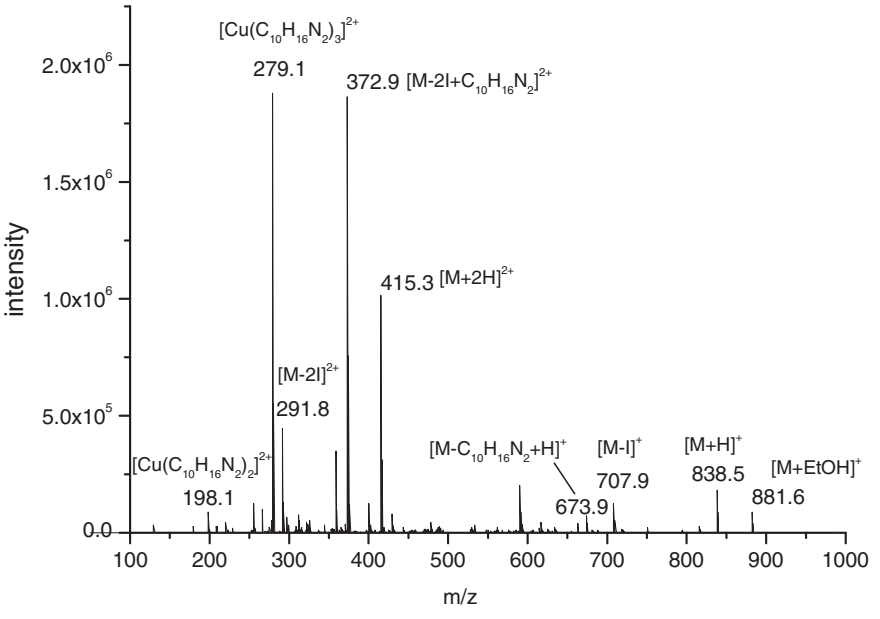

Figure 4. ESI-MS spectrum in the positive ion mode of a ethanol solution of $[C_{20}H_{32}Cu_2I_3N_4]_n$.

sensitivity of tryptophan to its local environment, changes in emission spectra of tryptophan are common in response to protein conformational transitions, subunit association, substrate binding, or denaturation [35]. Figure 5 shows the fluorescence emission spectra of BSA with various amounts of Cu(I/II) complex. It is obvious that BSA has a fluorescence emission peak at 347 nm. When different concentrations of the Cu(I/II) complex solution was titrated into a fixed concentration of BSA, a decrease in the fluorescence intensity of BSA was observed, indicating that there was an interaction between the Cu(I/II) complex and BSA. Furthermore, the maximum wavelength of BSA shifted from 347 to 345 nm after the addition of the Cu(I/II) complex, so a slight blue shift of the maximum emission wavelength of BSA was observed, suggesting that the microenvironment of tryptophan residues changed after the addition of the Cu(I/II) complex. Quantitative analysis of the binding of the Cu(I/II) complex to BSA was carried out using fluorescence quenching at 347 nm at different temperatures.

Fluorescence quenching is the decrease in the quantum yield for fluorescence from a fluorophore induced by a variety of molecular interactions with quencher molecules. Quenching can occur by different mechanisms, which are usually classified as dynamic quenching and static quenching. Dynamic quenching depends upon diffusion, where higher temperatures result in larger diffusion coefficients. As a result, the bimolecular quenching constants are expected to increase with increasing temperature. Static quenching refers to the formation of a ground state fluorophore–quencher complex, where increased temperature is likely to result in decreasing stability of the complexes, and thus lower values for the static quenching constants.

To clarify the fluorescence quenching mechanism of BSA by the Cu(I/II) complex, the procedure of the fluorescence quenching was first assumed to be a dynamic

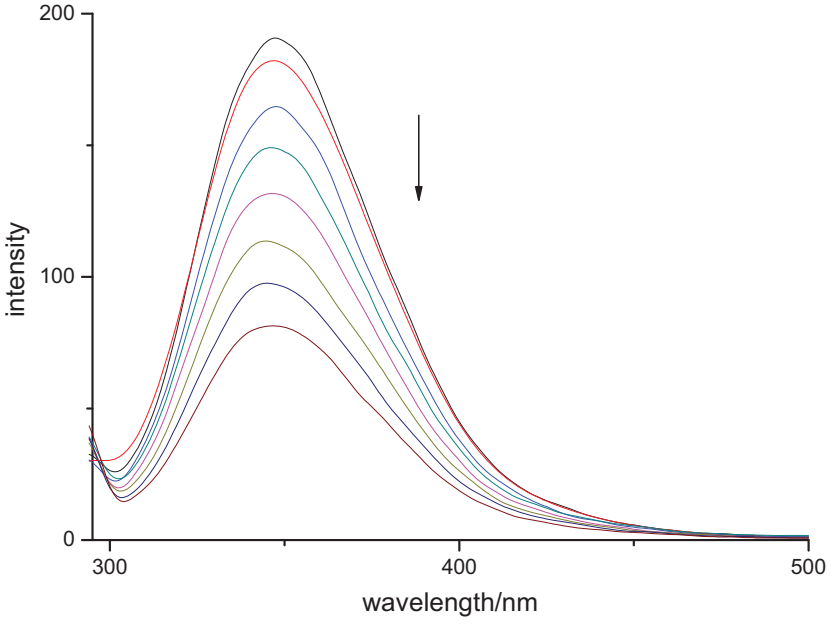

Figure 5. Emission spectra of BSA in the presence and absence of Cu(I/II) complex. [BSA]: 3×10^{-6}mol L^{-1}; [Cu(I/II) complex]: 0, 1, 2, 3, 4, 5, 6, 7×10^{-6}mol L^{-1}. $\lambda_{ex}=285$ nm; $\lambda_{em}=347$ nm; pH = 7.4; $T=293$ K.

quenching process; the fluorescence quenching data are usually analyzed by the Stern–Volmer equation:

$$F^0/F = 1 + K_q\tau_0[Q] = 1 + K_{sv}[Q]$$

where F^0 and F represent the fluorescence intensities in the absence and in the presence of the quencher, respectively. K_q is the quenching rate constant, K_{sv} is the dynamic quenching constant, τ_0 is the average lifetime of the biomolecule without quencher, and $[Q]$ is the concentration of quencher. Since the fluorescence lifetime of the biopolymer is 10^{-8} s [36], the quenching rate constant K_q can be calculated using the above equation. Stern–Volmer curves of F^0/F *versus* $[Q]$ at different temperatures are shown in figure 6 and the corresponding Stern–Volmer quenching constants K_{sv} are listed in table 3. The values of the Stern–Volmer quenching constants K_{sv} and K_q decrease with increase in temperature, and the values of K_q are much greater than the maximum scatter collision-quenching constant of the biomolecule (2.0×10^{10}mol L^{-1} s^{-1}) [8], indicating that the probable quenching mechanism of fluorescence of BSA by the Cu(I/II) complex is static quenching rather than dynamic collision.

3.3. *Binding constants and the number of binding sites*

For static quenching, the binding constant and the number of binding sites can be determined by the following equation [12]:

$$\log\left[(F^0 - F)/F\right] = \log K_b + n\log[Q]$$

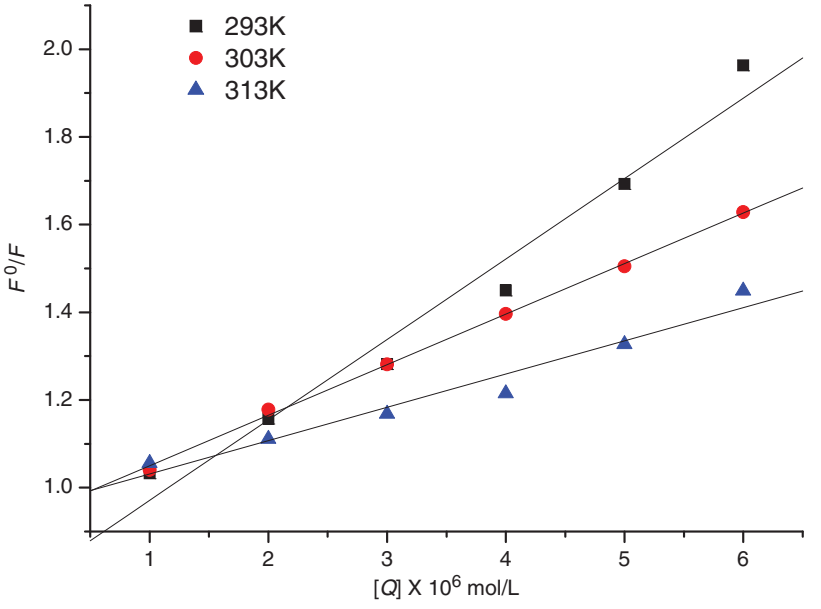

Figure 6. The Stern-Volmer plots for the interaction of Cu(I/II) complex with BSA.

Table 3. Stern–Volmer quenching constants, binding constants, binding points, and thermodynamic parameters of Cu(I/II)complex–BSA.

T (K)	K_{sv} (L mol^{-1})	K_q (L mol^{-1} s^{-1})	K_b (L mol^{-1})	n	ΔH (kJ mol^{-1})	ΔG (kJ mol^{-1})	ΔS (J mol^{-1} K^{-1})
293	1.84×10^5	1.84×10^{13}	5.95×10^8	1.68	−263.42	−49.56	−729.54
303	1.15×10^5	1.15×10^{13}	2.49×10^7	1.45		−42.26	
313	7.59×10^4	7.59×10^{12}	5.94×10^5	1.18		−34.96	

where K_b and n are the binding constant and the number of binding sites, respectively. According to this equation, the binding parameters can be obtained by a plot of the double-logarithm curve $\log[(F^0 - F)/F]$ *versus* $\log[Q]$ (figure 7). The values of K_b and n were calculated from the values of the intercept and slope of the plots, respectively, with results summarized in table 3. The Cu(I/II) complex binds to BSA and the binding constant decreases with increasing temperature, indicating that the stability of the Cu(I/II) complex–BSA system is reduced. The interactions are probably associated with hydrogen bonding and weakening of the complex–BSA stability. Values of n are 1–2, indicating that there are one or two classes of binding sites on BSA for the Cu(I/II) complex.

3.4. *Binding mode between the Cu(I/II) complex and BSA*

The interaction between the Cu(I/II) complex and BSA include hydrophobic forces, electrostatic forces, van der Waals interactions, and hydrogen bonds. The signs and magnitudes of the thermodynamic parameters determine the nature of the forces

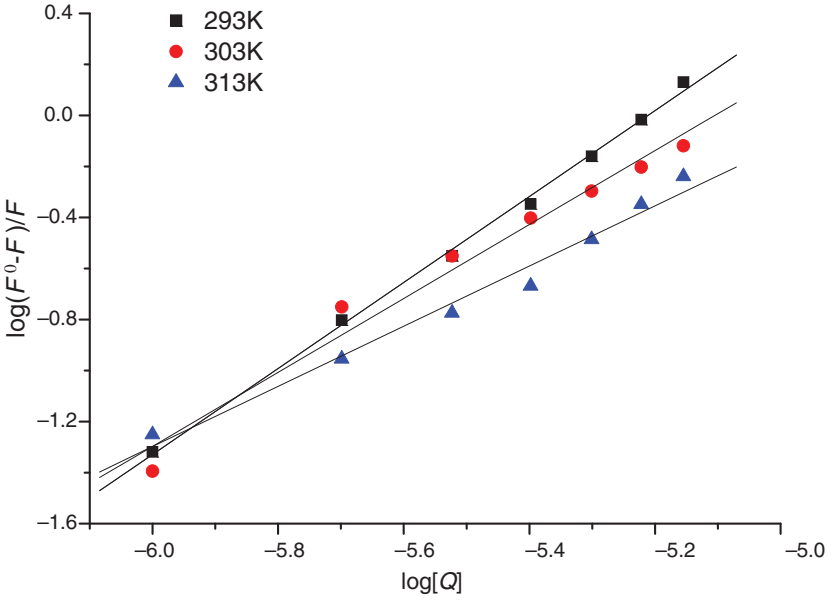

Figure 7. Plots of $\log(F^0-F)/F$ *vs.* $\log[Q]$.

actually taking part in the complex–BSA interaction. According to the ΔH and ΔS, the interaction between the Cu(I/II) complex and BSA can be concluded. If the temperature changes little, the reaction enthalpy change is regarded as a constant. In order to elucidate the interaction of Cu(I/II) complex with BSA, binding studies were carried out at 293, 303, and 313 K. The thermodynamic parameters were calculated from the van't Hoff equation and corresponding thermodynamically functions based on the temperature effect. The following two equations were used:

$$\ln K = -\frac{\Delta H}{RT} + \frac{\Delta S}{R}$$

$$\Delta G = -RT\ln K = \Delta H - T\Delta S$$

where R is the gas constant, T is the experimental temperature, and K is the binding constant at the corresponding T. The value of ΔH and ΔS were obtained from $\ln K$ *versus* $1/T$ plot (figure 8). The thermodynamic parameters for the interaction of the Cu(I/II) complex with BSA are shown in table 3. The binding constant of the Cu(I/II) complex–BSA decreases with increase in temperature, suggesting that the binding reaction of the Cu(I/II) complex with BSA is exothermic. According to the rules summarized by Ross and Subramanian [37], negative enthalpy and entropy values indicate that hydrogen bonds and van der Waals forces play a major role in the interaction of the Cu(I/II) complex with BSA.

3.5. *Synchronous fluorescence studies on Cu(I/II) complex binding to BSA*

The synchronous fluorescence of BSA can be used to study the environment of amino acid residues by measuring the possible shift in maximum emission wavelength, since such shifts reflect the changes of polarity around the chromophore. When the value

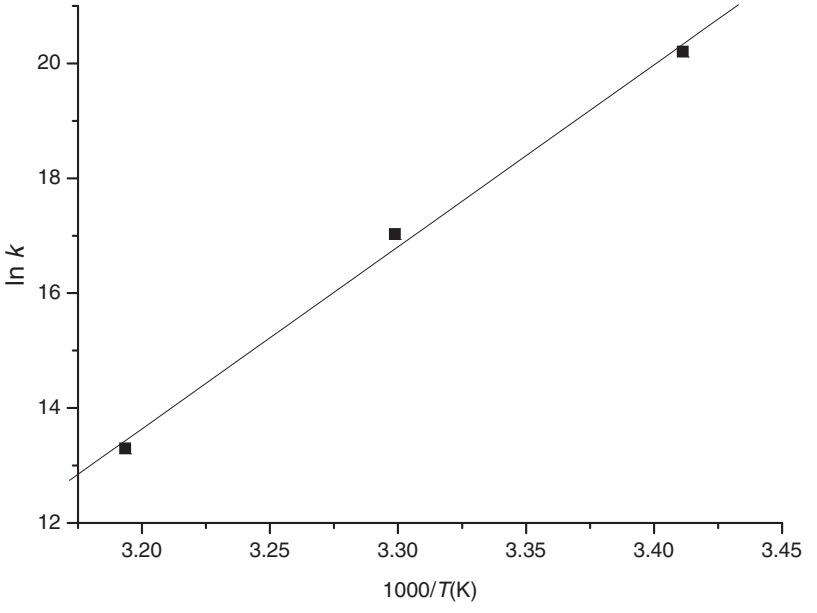

Figure 8. Van't Hoff plot for the interaction of BSA and Cu(I/II)complex.

($\Delta\lambda$) of the difference between excitation and emission wavelengths is fixed at 15 nm, synchronous fluorescence spectra only show information of the tyrosine residues, whereas when $\Delta\lambda$ is fixed at 60 nm, it provides the information of the tryptophan residues. Figure 9 presents the synchronous fluorescence spectra of BSA in the presence of the Cu(I/II) complex. When the Cu(I/II) complex was gradually added, the maximum emission wavelength of the tryptophan residues did not undergo a significant shift, suggesting that the interaction of the Cu(I/II) complex with BSA does not affect the polarity and conformation of the tryptophan residue micro-region. In contrast, an obvious blue shift was observed when $\Delta\lambda = 15$ nm, showing that the Cu(I/II) complex entered into the hydrophobic cavities and the conformation of BSA was changed. So we conclude that tyrosine residues participated in the molecular interaction between the Cu(I/II) complex and BSA.

3.6. *Energy transfer between the Cu(I/II) complex and BSA*

According to Förster's non-radiative energy transfer theory, the efficiency of energy transfer mainly depends on the following factors: (1) the extent of overlap between the fluorescence emission spectrum of the donor and the UV absorbance spectrum of the acceptor, (2) the orientation of the transition dipole of donor and acceptor, and (3) the distance between the donor and the acceptor is less than 8 nm. The overlap of the UV-Vis absorption spectrum of the Cu(I/II) complex with the fluorescence emission spectrum of BSA is shown in figure 10. The energy transfer efficiency is defined in the following equation:

$$E = 1/\left[1 + (r/R_0)^6\right] = 1 - \left(F/F^0\right)$$

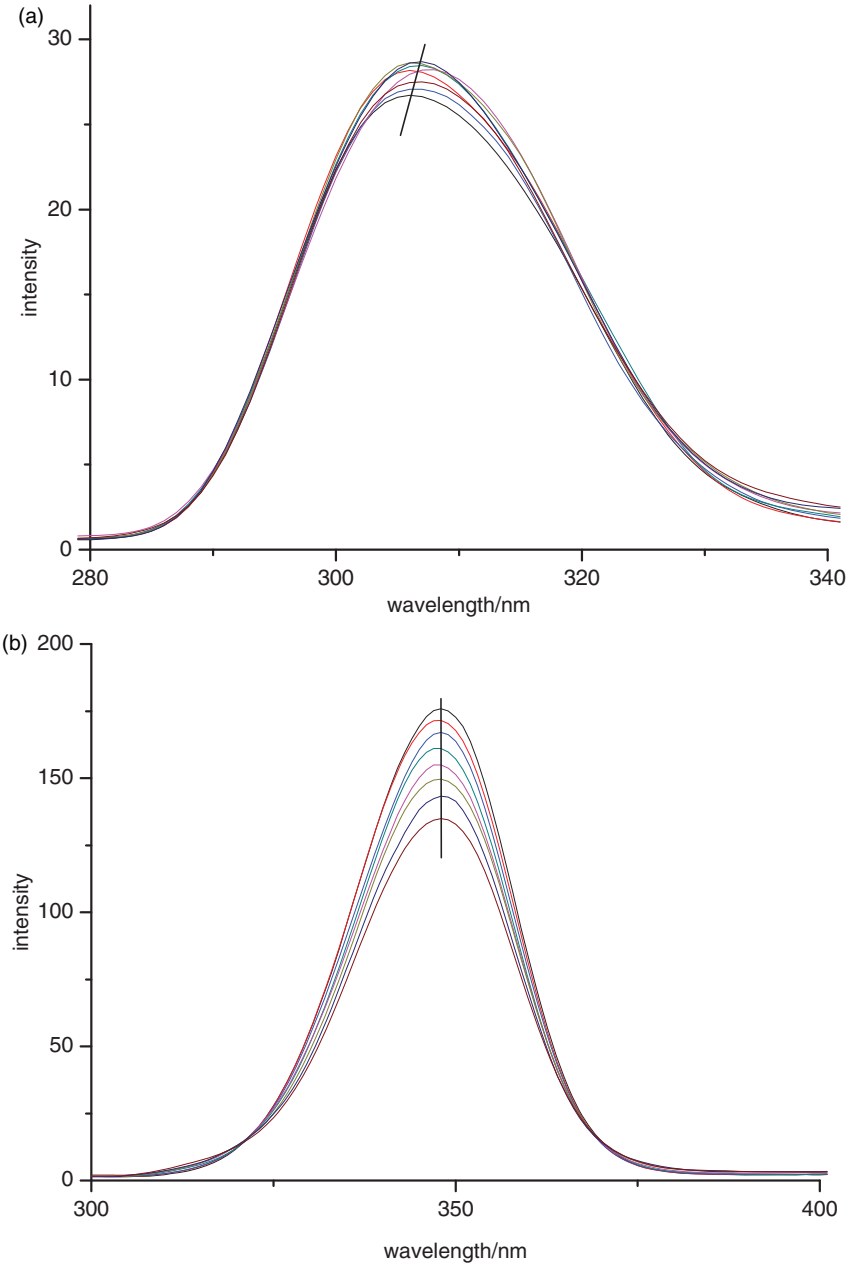

Figure 9. Synchronous fluorescence spectra of interaction between BSA and Cu(I/II) complex. (a) $\Delta\lambda = 15\,nm$; (b) $\Delta\lambda = 60\,nm$. [BSA]: $3\times10^{-6}\,mol\,L^{-1}$; [Cu(I/II) complex]: 0, 1, 2, 3, 4, 5, 6, $7\times10^{-6}\,mol\,L^{-1}$. pH = 7.4; $T = 303\,K$.

where E is the efficiency of energy transfer between the donor and the acceptor, F and F^0 are the fluorescence intensities of BSA in the presence and absence of the Cu(I/II) complex, r is the distance between the donor and the acceptor, and R_0 is the critical

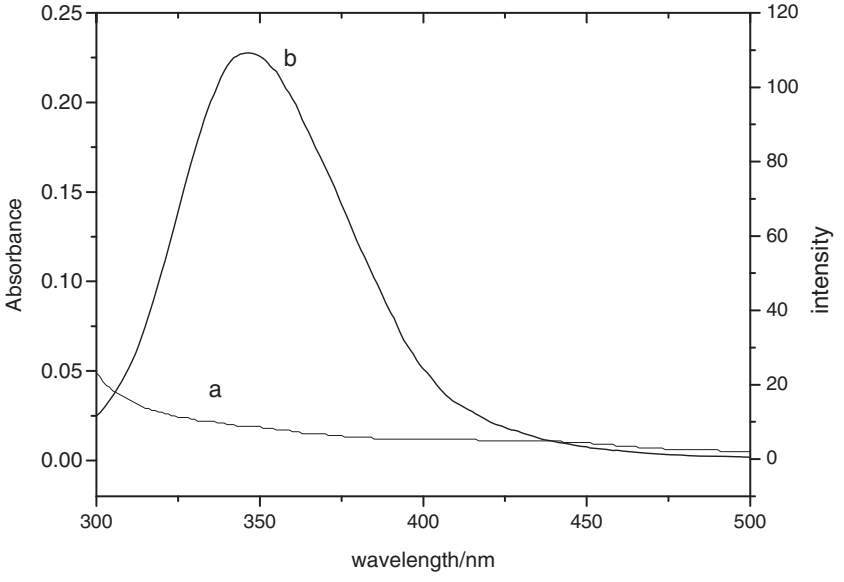

Figure 10. Spectral overlap of Cu(I/II) complex absorption (a) with BSA fluorescence (b) [BSA] = [Cu(I/II) complex]: 1×10^{-5} mol L^{-1} ($T = 293$ K).

distance at which transfer efficiency equals 50%. The value of R_0 can be calculated using the following equation:

$$R_0^6 = 8.79 \times 10^{-25}(K^2 \cdot N^{-4} \cdot \Phi \cdot J)$$

where K^2 is the spatial orientation factor of the dipole, N is the refractive index of the medium, Φ is the fluorescence quantum yield of the donor, and J is the overlap integral of the fluorescence emission spectrum of donor and absorption spectrum of the acceptor, which can be calculated by the following equation:

$$J = \frac{\int_0^\infty F(\lambda)\varepsilon(\lambda)\lambda^4 d\lambda}{\int_0^\infty F(\lambda)d\lambda}$$

where $F(\lambda)$ is the fluorescence intensity of the donor in the wavelength range λ to $\lambda + \Delta\lambda$ and $\varepsilon(\lambda)$ is the molar absorption coefficient of the acceptor at wavelength λ. In the present case, $K^2 = 2/3$, $N = 1.336$, $\Phi = 0.15$ [38]. From the overlapping spectrum, J can be evaluated by integrating the spectra for $\lambda = 300$–450 nm, $J = 2.82 \times 10^{-15}$ cm^3 L mol^{-1}, $E = 0.22$, $R_0 = 2.07$ nm, and $r = 2.56$ nm were calculated. Obviously, the donor–acceptor distance is less than 8 nm, and $0.5\,R_0 < r < 1.5\,R_0$, which implies a high possibility of energy transfer from BSA to the Cu(I/II) complex [7].

4. Conclusions

The crystal structure of the Cu(I/II) complex $[C_{20}H_{32}Cu_2I_3N_4]_n$ was determined by single-crystal X-ray diffraction. The interactions of the complex with BSA in

physiological buffer solution were studied by fluorescence spectroscopic methods. The results indicate that the Cu(I/II) complex is a strong quencher, and the decreasing values of the binding constants with increasing temperature indicate interaction with BSA through a static quenching procedure. The values of n revealed the presence of one or two classes of binding sites on BSA. The thermodynamic parameters of the binding interaction were determined and their values suggest that hydrogen bonds and van der Waals forces play a major role in interactions of the Cu(I/II) complex with BSA. The binding distance r between the Cu(I/II) complex and BSA indicates that energy transfer from BSA to the Cu(I/II) complex occurs. Synchronous fluorescence spectroscopy indicates that the conformation of BSA was changed in the presence of the Cu(I/II) complex.

Supplementary material

Crystallographic data for the structures in this article have been deposited with the Cambridge Crystallographic Data Center as supplementary publication CCDC No. 692706 for the title complex. Copies of the data can be obtained, free of charge, on application to CCDC, 12 Union Road, Cambridge CB2 1EZ, UK.

References

[1] G. Crisponi, V.M. Nurchi, D. Fanni, C. Gerosa, S. Nemolato, G. Faa. *Coord. Chem. Rev.*, **254**, 876 (2010).
[2] J.A. Drewry, P.T. Gunning. *Coord. Chem. Rev.*, **255**, 459 (2011).
[3] J.-Q. Lu, F. Jin, T.-Q. Sun, X.-W. Zhou. *Int. J. Biol. Macromol.*, **40**, 299 (2007).
[4] H.Y. Shrivastava, M. Kanthimathi, B.U. Nair. *Biochim. Biophys. Acta*, **1573**, 149 (2002).
[5] Y.-J. Hu, H.-G. Yu, J. Dong, X. Yang, Y. Liu. *Spectrochim. Acta, Part A*, **65**, 988 (2006).
[6] X.-J. Guo, X.-D. Sun, S.-K. Xu. *J. Mol. Struct.*, **931**, 55 (2009).
[7] P.N. Naik, S.A. Chimatadar, S.T. Nandibewoor. *J. Photochem. Photobiol. B*, **100**, 147 (2010).
[8] N. Shahabadi, M. Maghsudi. *J. Mol. Struct.*, **929**, 193 (2009).
[9] J.-N. Tian, J.-Q. Liu, Z.-D. Hu. *Bioorg. Med. Chem.*, **13**, 4124 (2005).
[10] T.-H. Wang, Z.-M. Zhao, B.-Z. Wei, L. Zhang, L. Ji. *J. Mol. Struct.*, **970**, 128 (2010).
[11] A. Mallick, B. Haldar, N. Chattopadhyay. *J. Phys. Chem. B*, **109**, 14683 (2005).
[12] Y.-L. Xiang, F.-Y. Wu. *Spectrochim. Acta, Part A*, **77**, 430 (2010).
[13] F. Dimiza, F. Perdih, V. Tangoulis, I. Turel, D.P. Kessissoglou, G. Psomas. *J. Inorg. Biochem.*, **105**, 476 (2011).
[14] Y.-Q. Wang, H.-M. Zhang, G.-C. Zhang. *J. Pharm. Biomed. Anal.*, **41**, 1041 (2006).
[15] G.-W. Zhang, A.-P. Wang, T. Jiang, J.-B. Guo. *J. Mol. Struct.*, **891**, 93 (2008).
[16] E. Karnaukhova. *Biochem. Pharmacol.*, **73**, 901 (2007).
[17] C.D. Kanakis, P.A. Tarantilis, M.G. Polissiou, S. Diamantoglou, H.A. Tajmir-Riahi. *J. Mol. Struct.*, **798**, 69 (2006).
[18] X.-J. Guo, L. Zhang, X.-D. Sun, X.-W. Han, C. Guo, P.-L. Kang. *J. Mol. Struct.*, **928**, 114 (2009).
[19] Z.-J. Cheng, Y.-T. Zhang. *J. Mol. Struct.*, **879**, 81 (2008).
[20] P.B. Kandagal, S.M.T. Shaikh, D.H. Manjunatha, J. Seetharamappa. *J. Photochem. Photobiol. A*, **189**, 121 (2007).
[21] D.M. Boghaei, S.S. Farvid, M. Gharagozlou. *Spectrochim. Acta, Part A*, **66**, 650 (2007).
[22] A.-Q. Gu, X.-S. Zhu, Y.-Y. Hu, S.-H. Yu. *Talanta*, **73**, 668 (2007).
[23] D. Dobrzynska, J. Janczak, A. Wojciechowska, K. Helios. *J. Mol. Struct.*, **973**, 62 (2010).
[24] F. Saczewski, E. Dziemidowicz-Borys, P.J. Bednarski, R. Grünert, M. Gdaniec. *J. Inorg. Biochem.*, **100**, 1389 (2006).
[25] D. Dobrzyńska, T. Lis, J. Woźniak, J. Jezierska, M. Duczmal, A. Wojciechowska. *Polyhedron*, **28**, 3150 (2009).

[26] G.M. Sheldrick. *SHELXS-97, Program of X-Ray Crystal Structure Solution*, University of Göttingen, Göttingen, Germany (1997).
[27] G.M. Sheldrick. *SHELXL-97, Program for X-Ray Crystal Structure Refinement*, University of Göttingen, Göttingen, Germany (1997).
[28] P.B. Durand, E.M. Holt. *Acta Cryst*., **C51**, 850 (1995).
[29] Y.-F. Song, G.A. Albada, M. Quesada, I. Mutikainen. *Inorg. Chem. Commun*., **8**, 975 (2005).
[30] Y. Li, K.-F. Yung, H.-S. Chan, W.-T. Wong. *Inorg. Chem. Commun*., **6**, 1451 (2003).
[31] C.-W. Lee, Z.-K. Chan, T.-R. Chen, J.-D. Chen. *Inorg. Chim. Acta*, **348**, 135 (2003).
[32] J.Y. Lu, A.B. Schauss, M. Julve. *Inorg. Chim. Acta*, **359**, 2565 (2006).
[33] P. Aslanidis, P.J. Cox, S. Divanidis, P. Karagiannidis. *Inorg. Chim. Acta*, **357**, 1063 (2004).
[34] R.-Z. Li, D. Li, X.-C. Huang, Z.-Y. Qi, X.-M. Chen. *Inorg. Chem. Commun*., **6**, 1017 (2003).
[35] Y.-Q. Wang, H.-M. Zhang, G.-C. Zhang, W.-H. Tao, Z.-H. Fei, Z.-T. Liu. *J. Pharm. Biomed. Anal*., **43**, 1869 (2007).
[36] F. Geng, L.-Q. Zheng, L. Yu, G.-Z. Li, C.-H. Tung. *Process Biochem*., **45**, 306 (2010).
[37] P.D. Ross, S. Subramanian. *Biochemistry*, **20**, 3096 (1981).
[38] S.M.T. Shaikh, J. Seetharamappa, P.B. Kandagal, S. Ashoka. *J. Mol. Struct*., **786**, 46 (2006).